

PACS numbers: 42.65.Jx; 42.65.Re
DOI: 10.1070/QE2015v045n04ABEH015640

Comparative analysis of post-focal filamentation of focused UV and IR laser pulses in air

Yu.E. Geints, A.A. Zemlyanov, A.A. Ionin, D.V. Mokrousova, L.V. Seleznev, D.V. Sinitsyn, E.S. Sunchugasheva

Abstract. **We report the results of laboratory experiments and numerical calculations of the spatial position and structure of a plasma channel produced in air by high-power focused femtosecond laser radiation with wavelengths of 740 and 248 nm as a result of its self-focusing and filamentation. A comparative analysis of the physical patterns of filamentation of IR and UV laser beams with variations in the beam focal length, transverse size and power is performed. It is found that a plasma channel beyond the linear focal waist of the laser beam is formed differently for two different spectral ranges.**

Keywords: *ultrashort laser radiation, focusing, self-focusing, filamentation.*

1. Introduction

The self-action of high-power ultrashort laser pulses propagating in a gas medium occurs generally in the filamentation regime [1–4]. The main physical factors leading to filamentation are the Kerr optical effect, which causes beam self-focusing, as well as gas ionisation and formation of a plasma channel in the medium. Filamentation is accompanied by large-scale self-phase modulation of a pulsed laser beam propagating in a nonlinear medium, which leads to spatial and temporal fragmentation of the laser pulse into localised regions: filaments with a quasi-constant (on a rather long path segment) peak intensity and a transverse size. For example, for a laser pulse with a carrier wavelength of 800 nm, the peak intensity in the filamentation zone in air is $\sim$50 TW cm^{-2} at a filament diameter on the order of several hundreds of micrometers [4].

To date, the scenario of filamentation of a high-power femtosecond pulse in different media has been thoroughly elaborated; its detailed description can be found, for example, in [1–4]. One of the key points in this scenario is the formation of ionised plasma regions in the light-beam channel under a strong optical field; these regions accompany the laser pulse, simultaneously stabilising intensity in light filaments. Since the characteristic lifetime of laser plasma in air is more than several hundreds of picoseconds [5], the rather short femtosecond laser pulse leaves a trace of ionised gas, where the free-charge density is maximal in the filamentation zone. The internal structure of this plasma channel depends on the filamentation regime (single or multiple) and can be rather complex in both longitudinal and transverse directions [6–8].

An important problem is to determine the spatial position of the plasma channel on the propagation path. The beginning of the beam filamentation zone can be calculated fairly exactly (at least in laboratory studies) using the well-known Marburger formula [1]. At the same time, the final coordinate of the plasma channel is generally uncertain; it depends on a number of factors (instability of laser beam parameters and influence of optical elements). This problem can be solved by geometric focusing of the laser beam [9]. Note that the use of a laser pulse guarantees the formation of a plasma channel before the geometric focus of the guiding optics, while the filamentation generally comes to an end within the linear focal waist of the laser beam due to its strong angular divergence after the waist [10, 11].

However, it was found that, under certain conditions (mainly for narrow focused beams), a filament may pass through the linear focus; i.e., filamentation is also observed behind the focal waist of the guiding optical system. For a near-IR laser beam propagating in air, this regime was experimentally observed for the first time in [12]. Then it was investigated in detail in [13] by measuring the longitudinal profile of a fluorescence signal emitted by nitrogen in which a femtosecond Ti:sapphire laser pulse (λ = 800 nm) was self-focused. Here, along with one expected fluorescence intensity peak (corresponding to the initial coordinate pulse of self-focusing), another peak was observed behind the linear lens focus. Talebpour et al. [13] referred to this effect as nonlinear refocusing behind the linear focus (post-focal refocusing).

Note that the term "nonlinear light refocusing" was introduced in [14], where filamentation of a collimated light beam of supercritical power in air was investigated and nonmonotonic behaviour of the paraxial light energy density on the propagation path was experimentally observed for the first time. The occurrence of this multimodal longitudinal energy density profile was explained (within the model of moving foci [15]) by nonlinear transformations of the laser pulse temporal profile as a result of refraction from self-induced plasma.

A detailed theoretical interpretation of post-focal refocusing [16] revealed that, under certain conditions, a light filament (and, therefore, plasma channel) can be both self-recovered

Yu.E. Geints, A.A. Zemlyanov V.E. Zuev Institute of Atmospheric Optics, Siberian Branch, Russian Academy of Sciences, pl. Akad. Zueva 1, 634021 Tomsk, Russia; e-mail: ygeints@iao.ru;
A.A. Ionin, L.V. Seleznev, D.V. Sinitsyn P.N. Lebedev Physics Institute, Russian Academy of Sciences, Leninsky prosp. 53, 119991 Moscow, Russia;
D.V. Mokrousova, E.S. Sunchugasheva P.N. Lebedev Physics Institute, Russian Academy of Sciences, Leninsky prosp. 53, 119991 Moscow, Russia; Moscow Institute of Physics and Technology (State University), Institutskii per. 9, 141700 Dolgoprudnyi, Moscow region, Russia

Received 23 July 2014; revision received 16 September 2014
Kvantovaya Elektronika **45** (4) 321–329 (2015)
Translated by Yu.P. Sin'kov

behind the linear focal beam waist and continuously pass ("extend" [17]) behind the waist without visible refocusing. In terms of the physical scenario of filamentation [1], implementation of these conditions corresponds to successful suppression of the laser beam angular divergence (caused by diffraction behind the focus and defocusing in the self-induced plasma) by Kerr self-focusing.

Filaments can also pass behind the linear focus of the system when the initial Gaussian profile of the beam is changed by superposition of amplitude diaphragms of different shapes [18]; however, this approach calls for additional alignment and changes significantly the beam filamentation.

At the same time, the aforementioned studies were performed for only one light wavelength in the near-IR range. In our opinion, it is important to consider the possibility of implementing post-focal laser beam filamentation in another spectral range, because the optical nonlinearity of air depends on the light wavelength [19]; this dependence may add some new features to the self-action dynamics of a focused laser beam.

This study, on the one hand, continues the investigations of filamentation of a femtosecond laser pulse behind the focus of the optical system, which were started in [16]. On the other hand, it supplements the study of the filamentation of IR and UV laser beams upon focusing [18]. We present the results of the experiments aimed at establishing the regularities of the formation of a plasma channel in the vicinity of the geometric focus of the optical system during filamentation of laser beams with two wavelengths: in the near-IR and UV spectral regions (the main and third harmonics of Ti:sapphire laser radiation). A comparative analysis of the spatial position of the laser-induced plasma region and the behaviour of the electron density in it with variation in the focal length, laser beam size and laser pulse power is performed based on measuring the linear plasma electron density and corresponding theoretical simulation for the two wavelengths. The physical factors causing the observed differences in the dynamics of post-focal filamentation of laser beams with different wavelengths are discussed.

2. Experimental results

The parameters of plasma channels formed upon propagation of focused femtosecond pulses were experimentaally studied using a femtosecond 'Start' Ti:sapphire laser system, which generates laser pulses with a repetition rate of 10 Hz at wavelengths of 248 and 740 nm. The pulse width (FWHM) was 100 fs. A schematic of the experiment is presented in Fig. 1. After passing through binary attenuator (*2*), a laser beam is focused by thin fused silica lens (*3*). An electric system with two hemispherical electrodes (*4*) (hemisphere diameter 20 mm, interelectrode distance $R_\perp$ = 3 mm) was installed on the laser beam path to measure the electron density distribution in the laser plasma channels of beam filaments. The formation of plasma changed the capacitance of the capacitor formed by the electrodes, and the capacitor recharge current was recorded using oscilloscope (*5*). The measured capacitor recharge current is proportional to the linear plasma density in the channel, because variation in capacitance depends on the electron density and the length and width of the plasma channel between the spheres. Moving electrodes along the optical axis, we measured the linear plasma density along the channel.

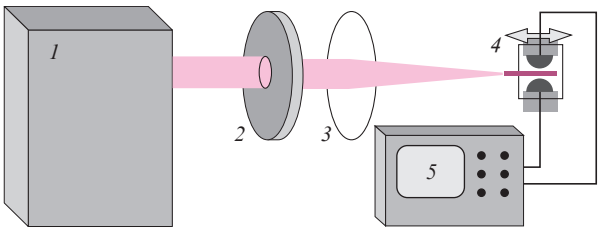

Figure 1. Schematic of the experiment:
(*1*) femtosecond 'Start' Ti:sapphire laser system; (*2*) attenuator; (*3*) lens; (*4*) movable system of electrodes; (*5*) oscilloscope.

The experiments were performed in several stages. In the first series of measurements, we analysed the influence of the focusing-system optical power on the spatial position of the filamentation zone and the character of its change in the axial direction. To this end, we used UV and IR laser beams with approximately equal initial diameters: $d_0 \sim 4$ and ~ 6 mm (at the 1/e level) for the UV and IR beams, respectively, and relative power η_0 (see below). The focal length f of the guiding optics was varied. Figure 2 shows the corresponding data for a set of f and η_0 values.

The electric signal U_d, arising in the air gap between the electrodes as a result of their displacement along the laser beam optical path, is evidently proportional to the density ρ_{ez}, $U_d \propto \rho_{ez}$ (compare Figs 3a and 3b), where

$$\rho_{ez}(z) = \iint_{\boldsymbol{R}_\perp} \rho_e(x,y,z)\,\mathrm{d}\boldsymbol{r}_\perp ,$$

and ρ_e is the laser plasma free-electron density (the integration is over the transverse coordinates in the spatial region $\boldsymbol{r}_\perp \in \boldsymbol{R}_\perp$). Hence, we will use below the ρ_{ez} value. Densities ρ_{ez} in Fig. 2 are presented for the propagation of laser pulses with λ_0 = 740 nm and initial energies E_0 = 1.4 and 2.8 mJ and pulses with λ_0 = 248 nm and E_0 = 0.09 and 0.18 mJ. The symbols in the curves are the results of arithmetic averaging of the results of individual measurements over a series of independent laser shots. The rms spread of ρ_{ez} values did not exceed 10%.

In the theory of light wave self-focusing [1, 11], the measure of the optical power of cubic (Kerr) nonlinearity of the medium is the relative (reduced) radiation power $\eta_0 = P_0/P_c(\lambda_0)$, where $P_c = \lambda_0^2/(2\pi n_0 n_2)$ is the critical self-focusing power and n_0 and n_2 are, respectively, the linear refractive index of the medium and the factor at cubic nonlinearity. If we assume that the n_2 values for air in the IR and UV ranges are, respectively, 3.2×10^{-23} m^2 W^{-1} (λ_0 = 740 nm) [2] and 8.0×10^{-23} m^2 W^{-1} (λ_0 = 248 nm) [18], the critical powers P_c are, respectively, 3.18 and 0.12 GW. Specifically this decrease in the P_c value for short wavelengths provided approximately the same range of variation in relative power η_0 for UV and IR pulses in our measurements.

Let us first consider Figs 2a and 2b, which present the data on filamentation of IR pulses. It can be seen that an increase in the laser pulse power displaces the beginning of the plasma region (which is considered to be an indicator of beam filamentation) towards smaller longitudinal coordinates z; this is due to the laser beam self-focusing. Depending on the lens optical power, the right boundary of the plasma channel can be either within (Fig. 2b) or beyond the linear focal waist of the beam (Fig. 2a). The linear sizes and position of the focal waist can be estimated based on the longitudinal profiles of relative radiation intensity $I(z)$ (Fig. 2), which were cal-

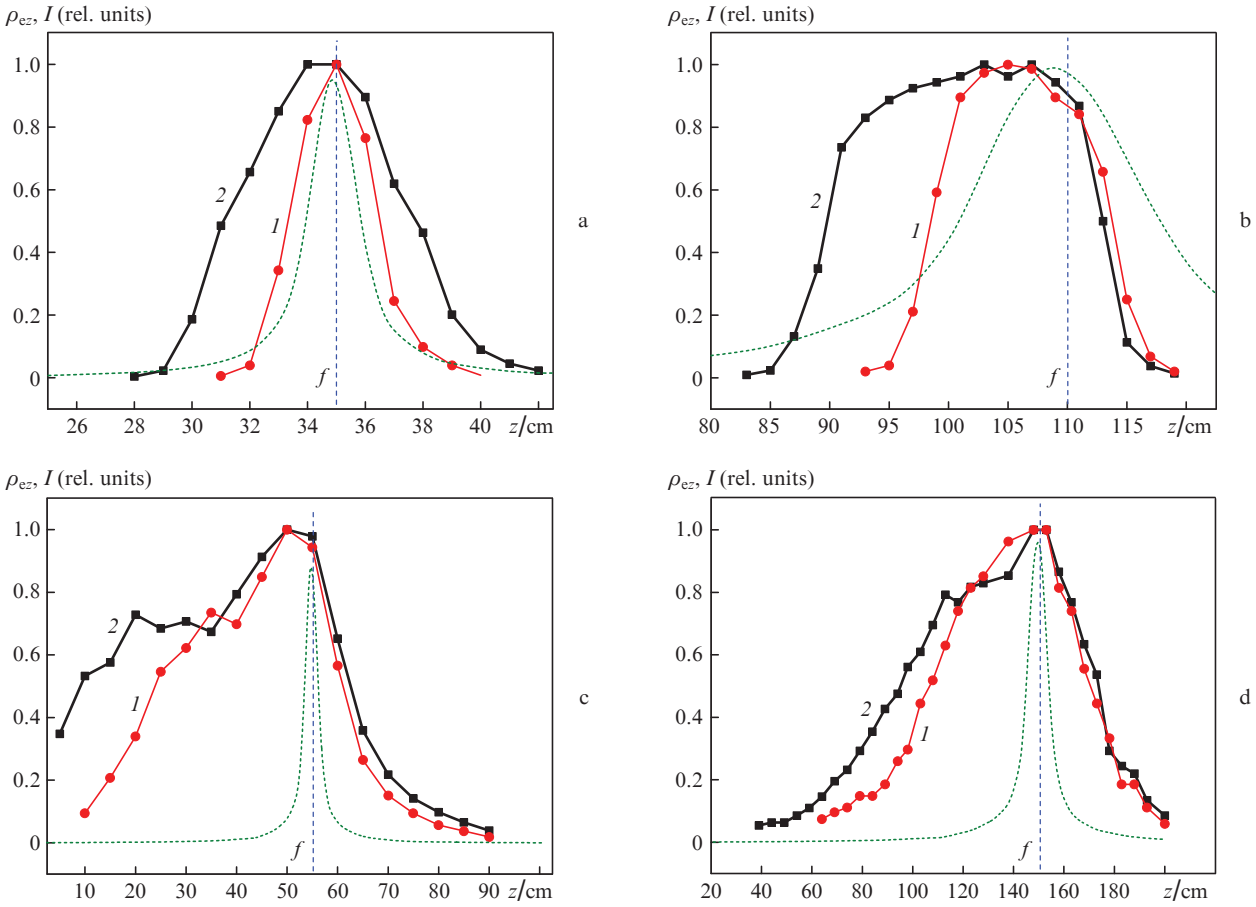

Figure 2. Linear plasma electron density in the (a, b) IR- and (c, d) UV-beam filamentation zones at different focal lengths and pulse powers $\eta_0 =$ (*1*) 10 and (*2*) 20. The dashed line shows the relative laser radiation intensity I in the linear regime. Hereinafter (Figs 3–6), the vertical line shows the position of the geometric focus of the mirror or lens.

culated for the case of focused propagation in vacuum (the intensity values were normalised to the intensity at the focal point).

As was shown in [16], the filament passage through the beam geometric focus corresponds to the case where the optical power of the focusing Kerr lens, $\vartheta_n = \sqrt{\eta_0 - 1}/L_p$, dominates over the diffraction divergence behind the focal plane with equivalent optical power $\vartheta_f = 1/f$:

$$\vartheta_n > \vartheta_f. \qquad (1)$$

Here, $L_p = \pi d_0^2/(2\lambda_0)$ is the free diffraction length of the beam. Using the results of this study, we find that the IR-beam filament (Fig. 2a) formed before the linear focus of the optical system can pass through the focal waist under the condition $\eta_0 > 17$. This inequality corresponds to the situation described by curve (*2*) in Fig. 2.

The filamentation zone for a weakly focused beam (Fig. 2b), despite the evident validity of condition (1), is limited from the right by the beam focal waist. This is evidenced by a virtually identical decrease in the relative electron density in the plasma channel with an increase in the coordinate, independent of the pulse power. It can be seen that in this case the peak linear density follows the decrease in the laser intensity in the linear focus, thus outlining the beam waist. This is caused by a significant increase in the length of the filamentation zone to the linear focus, which leads to a corresponding rise in the angular divergence of the beam as a whole (due to the nonlinear transformations of its spatial spectrum [1]) before it reaches the focal plane of the lens. Therefore, to compensate for this additional divergence and provide filamentation behind the focal waist, one must use radiation with a higher peak power in pulse than that applied in the experiments discussed here.

Let us now consider the filamentation of a UV laser beam (Figs 2c, 2d). One can see that post-focal filamentation of a beam with neither tight nor soft focusing was experimentally observed. This is evidenced (Fig. 2b) by virtually invariable (independent of pulse energy) position of the plasma right boundary. Note that the absolute values of linear electron densities in the plasma channel formed by a UV laser beam are generally several times larger than the corresponding values for IR-beam filamentation.

Inequality (1) explains why post-focal filamentation cannot occur with a decrease in the radiation wavelength, with other factors (beam size and power) being equal. The case is that the diffraction length L_d increases for UV radiation, i.e., the ϑ_n value in the left-hand side of (1) decreases. An evident solution to this problem is to increase the focal length f of the optical system. Nevertheless, a further increase in f in our experiments [as, for example, for a long-focal-length mirror (Fig. 3, $f = 520$ cm)] also did not lead to post-focal filamentation of the UV pulse. The plasma regions formed as a result of beam filamentation, depending on the pulse energy, had a

length of about 3–4 m and different linear free-charge densities (Fig. 3a). However, the arrangement of plasma channels near the focal plane was the same as for a more tightly focused beam and as in the above-considered case of long-focal-length lens and fundamental laser radiation harmonic (see Fig. 2b). Note that, in terms of this criterion for passage through the focus (1), an increase in the focal length of the guiding optics completely compensated for the almost tenfold increase in the diffraction length of laser beam when the third harmonic was used.

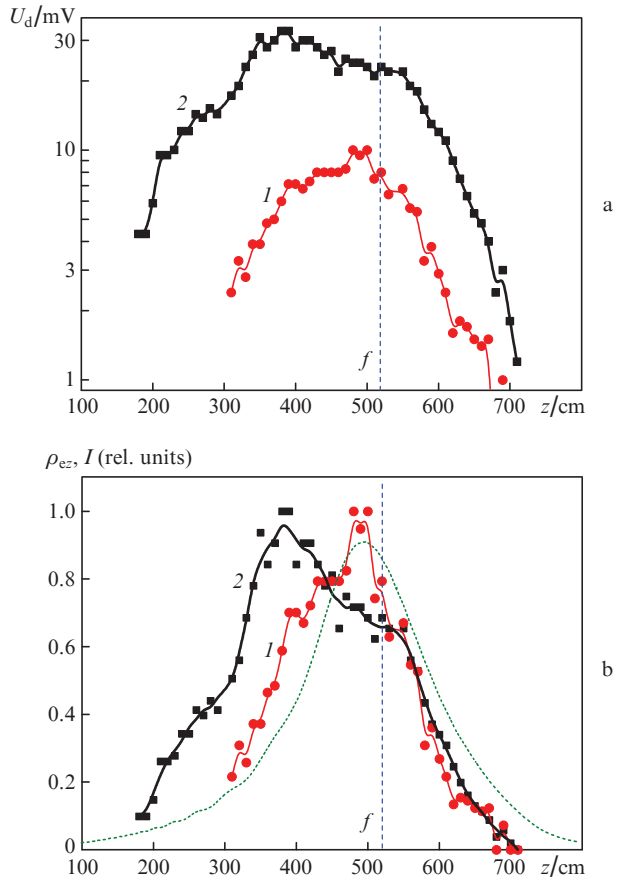

Figure 3. Dependences of (a) the electric signal magnitude U_d in the air gap and (b) the relative linear plasma density ρ_{ez} on filamentation of UV pulses with energies E_0 = (*1*) 74 and (*2*) 160 μJ at focal length f = 520 cm. The dashed line shows the relative laser radiation I in the linear mode.

In the next stage of our experiments, which were aimed at obtaining filamentation behind the geometric focus, we changed the initial size of the light beam to facilitate the formation of post-focal filament. Indeed, considering expression (1), one can easily make sure that, if power P_0 and diffraction length L_d are expressed in terms of other pulse parameters, the ratio of the optical powers of Kerr focusing and diffraction behind the linear focus are inversely proportional to the beam diameter d_0: $\vartheta_n/\vartheta_f \propto 1/d_0$. Thus, reducing the light-beam cross section, one can satisfy the criterion for beam refocusing behind the focus.

To this end, we used a set of circular diaphragms with a fixed hole diameter and an iris diaphragm with a gradually varied aperture, which were placed directly after the point of laser beam emergence from the diffraction compressor. The application of the diffraction attenuator and diaphragms with different sizes allowed us to obtain laser beams of different diameters but with the same energy in some cases. The results of measuring the linear electron density in the plasma channel formed by two light beams with different wavelengths are shown in Fig. 4. In both cases the focal length was fixed to be 50 cm, whereas the beam diameter and energy were varied. Let us consider these results in detail.

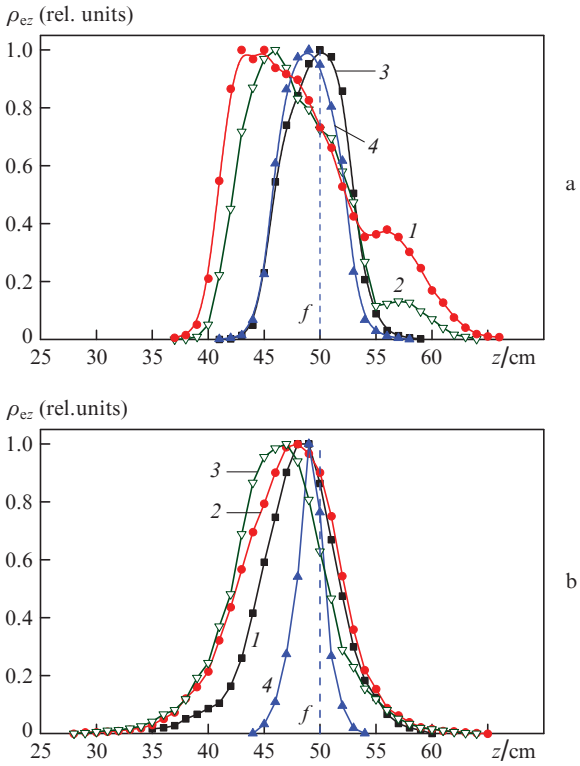

Figure 4. Linear plasma electron density in the (a) IR- and (b) UV-beam filamentation zones for beams with different diameters d_0 and pulse energies E_0. (a) d_0 = 2.5 mm, E_0 = 1.2 mJ (*1*); d_0 = 3 mm, E_0 = 1.7 mJ (*2*); d_0 = 8 mm, E_0 = 1.7 mJ (*3*); and d_0 = 4.8 mm, E_0 = 1.2 mJ (*4*). (b) d_0 = 1.6 mm, E_0 = 48 μJ (*1*), d_0 = 5 mm, E_0 = 240 μJ (*2*), d_0 = 2.7 mm, E_0 = 140 μJ (*3*), and d_0 = 5 mm, E_0 = 40 μJ (*4*). Curves (*1*,*2*) and (*3*,*4*) correspond, respectively, to the presence and absence of post-focal filamentation.

Note that, under certain conditions, one can speak about implementation of post-focal filamentation of laser radiation in both spectral ranges; practically in all cases reduction of the light-beam diameter leads to this effect. For example, one can compare curves (*1*) and (*4*) in Figs 4a and 4b, which correspond to laser pulses with close energies (and, therefore, powers) but differing beam cross sections. The versions presented by curves (*1*) correspond to the passage of plasma channel through the focal waist, while the versions presented by curves (*4*) correspond to the absence of filamentation, because the experimentally measured profile of the linear plasma density almost coincides with the laser beam intensity profile calculated for linear-focusing conditions (not shown in the figures).

In the case of UV pulse [Fig. 4b, curve (*2*)], passage of the plasma region behind focal waist was also implemented for a wide beam with diameter d_0 = 5 mm. However, the pulse energy was maximum in this case: E_0 = 240 μJ, a value cor-

responding to an excess by a factor of about 35 above the threshold power P_c at this wavelength. A decrease in the radiation power by less than half [curve (*3*)] stops the filament, impeding its propagation behind the waist.

Comparison of Figs 4a and 4b reveals some differences in the character of post-focal filamentation for IR and UV pulses. The short-wavelength laser beam forms a plasma channel, which extends behind the beam geometric focus [16, 20], whereas the IR-beam filamentation demonstrates pronounced refocusing [Fig. 4a, curves (*1*, *2*)], when the electron density in the plasma region behind the focus first decreases and then rises again to form the second local peak. Recall that in the above-cited study [13] experimental observation of refocusings upon filamentation of tightly focused femtosecond 800-nm laser beam was performed using much higher power laser pulses (with energy of several tens of millijoules) than in our experiments.

Note that only an increase in the laser beam power may be insufficient to implement axial refocusing behind the geometric focus of the beam, because this increment in power primarily removes the filament beginning from the focal plane and increases the nonlinear beam divergence before the focus (see Fig. 2b). It is necessary to implement conditions under which a filament would start near the linear focal waist but the pulse power would be sufficient to overcome the geometric divergence of the axial energy-bearing beam component behind the focus. These conditions correspond specifically to the case of narrow (the d_0/f ratio is small) and high-power ($\eta_0 \gg 1$) laser beams.

The refocusing of the initially focused laser beam is considered here as a manifestation of nonlinearity of the medium; it is related to the repeated beam filamentation behind the linear focus. This process may also occur as a result of the formation of a new plasma channel behind the focus when multiple filamentation of a previously focused beam is implemented [21, 22]. This regime is observed when the laser pulse power greatly exceeds (generally by an order of magnitude) the critical value P_c; apparently, it is described by the curve with the highest UV pulse energy in Fig. 4b. Multiple filamentation leads to simultaneous formation of several high-intensity light structures in different regions of the beam cross section.

Since the transverse profile of the laser beam intensity for both harmonics differs from unimodal, the beam filamentation is likely multiple (at least when the peak power η_0 exceeds 10). At the same time, as was shown in [23], multiple filamentation of a tightly focused beam is characterised by the same properties as the formation of a single filament. Specifically, there is some threshold degree of beam focusing (or threshold beam power), the intersection of which recovers or breaks up the filamentation behind the focal waist. Moreover, spatial harmonics of laser radiation are filtered in the linear focus of the optical system, which regularises the random fragmentation of the light beam behind the focus and reduces the number of off-axis filaments. Therefore, in our further analysis, we will not intentionally separate the cases of single or multiple filamentation.

3. Numerical simulation

To study in more detail the dynamics of post-focal filamentation of UV and IR light, we numerically simulated the propagation of focused pulsed Ti:sapphire laser beams at the first and third harmonics in air. The simulation was based on solving the nonlinear Schrödinger equation for the envelope of the electric field strength of the light wave. Numerous studies (see, for example, reviews [1–4]) showed that the nonlinear Schrödinger equation adequately describes all significant linear and nonlinear processes related to the propagation of a laser pulse (with a duration of at least no less than several optical periods) in a medium. The linear part of the nonlinear Schrödinger equation takes into account the dispersion of the laser pulse group velocity and the beam diffraction. The model of air optical nonlinearity included the instantaneous and inertial components of the Kerr effect and the change in the complex refractive index of the medium caused by the photoionisation of air molecules. The photoionisation rate was calculated according to the Popov–Perelomov–Terent'ev ionisation model [23]. The formulation of the nonlinear Schrödinger equation and velocity equation for the instantaneous free-electron density in the plasma region and details of numerical solution can be found, for example, in [16].

The initial laser beam in the numerical calculation was set in the form of a focused Gaussian (in both spatial and temporal coordinates) beam with a variable initial radius R_0, radius of phase front curvature f and peak pulse power P_0. The initial pulse duration t_p was fixed in the calculations and corresponded to the experimentally implemented value. We used the cylindrically symmetric version of the program code.

Figure 5 shows a longitudinal profile of the linear electron density ρ_{ez} in the plasma channel on the light beam axis, formed as a result of air photoionisation during filamentation

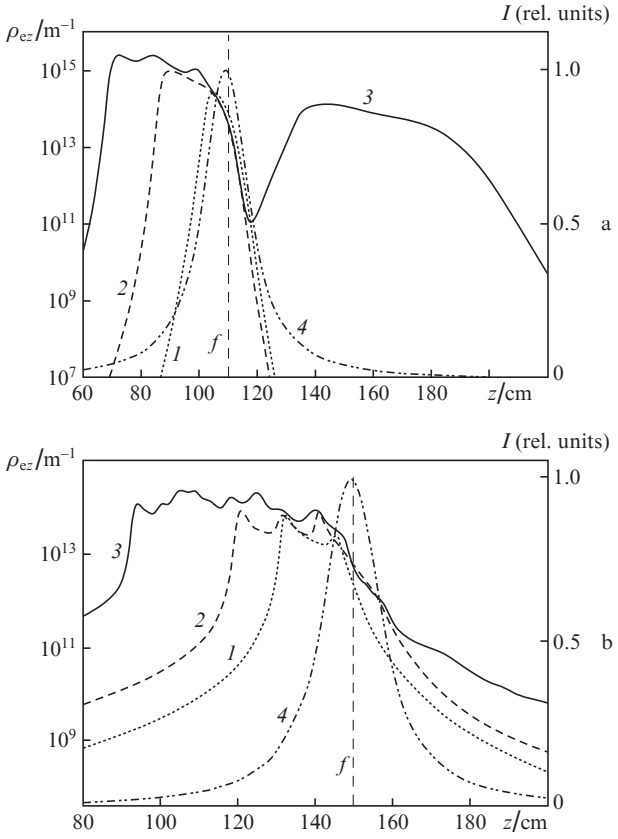

Figure 5. Linear plasma free-electron density ρ_{ez} obtained by simulating filamentation of (a) IR and (b) UV laser pulses in air with energies (a) E_0 = (*1*) 1.4, (*2*) 2.8 and (*3*) 5.6 mJ and (b) (*1*) 90, (*2*) 180 and (*3*) 320 μJ. Curve (*4*) shows the relative intensity I in the linear regime.

for the situations depicted in Figs 2b and 2d. The parameter $\rho_{ez}(z)$ was calculated by integrating over the three-dimensional distribution of the bulk free-electron density $\rho_e(r_\perp, z)$ (formed by the end of the laser pulse) over the transverse coordinate $\boldsymbol{r}_\perp$.

The ρ_{ez} profiles in Fig. 5 are in good qualitative agreement with the experimental data obtained in the range of pulse energies under study [curves (*1*) and (*2*)]; they indicate the absence of any significant plasma formation (and, therefore, filamentation) behind the light-beam focal plane. An increase in parameter E_0 only shifts the left boundary of the plasma channel (beam filament) to the origin of coordinates, while the post-focal evolution of the plasma region remains similar for different E_0 values.

Nevertheless, one can implement filamentation behind the focal waist in calculations by choosing a higher (than in experiments) energy of model pulse radiation [curve (*3*)]. In this case, the IR beam undergoes pronounced refocusing and repeated filamentation, while the plasma channel of UV filament is continuously extended behind the focal waist.

Before the geometric focus the peak values of linear electron density in the plasma channel in the IR laser-beam filamentation zone are approximately an order of magnitude larger than for the UV laser beam. At the same time, for the IR beam, the absolute peak plasma density ρ_{em} in filaments is 3×10^{23} m^{-3}; this value exceeds the corresponding value for the plasma of the UV-beam filament ($\sim10^{24}$ m^{-3}) by a factor of more than three. Obviously, the reason is in the smaller transverse size of the filament for the UV beam [24], which forms a narrower plasma channel. According to the calculation results, this channel had a virtually constant average width $d_f \approx 50$ μm (at the level $\rho_{em} = 10^{21}$ m^{-3}) on the entire filamentation length. At the same time, the width of the IR-filament plasma channel before the focus oscillates in the range of 150–200 μm. Behind the focal plane (in the region of IR-pulse refocusing), the plasma-channel width sharply decreases and reaches the value characteristic of the UV filament ($d_f \approx 80$ μm), which leads to a decrease in the linear free-electron density in the secondary filament by an order of magnitude (Fig. 5a).

The differences in the filamentation dynamics for IR and UV laser beams are most pronounced in Figs 6a and 6b, which show a time scan of laser pulse intensity $I(0, z, t)/I_0$ during pulse propagation in the medium in the form of a continuous-tone image. Here, $I_0 = P_0/(\pi R_0^2)$ is the initial peak intensity, and the transverse coordinate r is chosen to lie on the beam axis ($r = 0$). The relative time t/t_p is counted from the pulse centre; thus, negative and positive time values correspond to the pulse leading and trailing edges, respectively.

Figures 6a and 6b demonstrate that the optical field of both UV and IR beams undergoes local focusing in different time intervals: one can see many intensity peaks, which sometimes merge into strong bands. Specifically a set of these local temporal peaks at each point of the optical path forms a light filament [15], which can experimentally be recorded by a photodetector. Figures 6c and 6d show for clearness profiles of axial energy density $w(r = 0, z)/w_0$ along the path, calculated by integrating the spatial and temporal intensity distributions in the corresponding panels over time.

There are some qualitative differences in the images presented in Fig. 6. In contrast to the IR beam, the UV beam undergoes much more temporal focusings, and they all occur

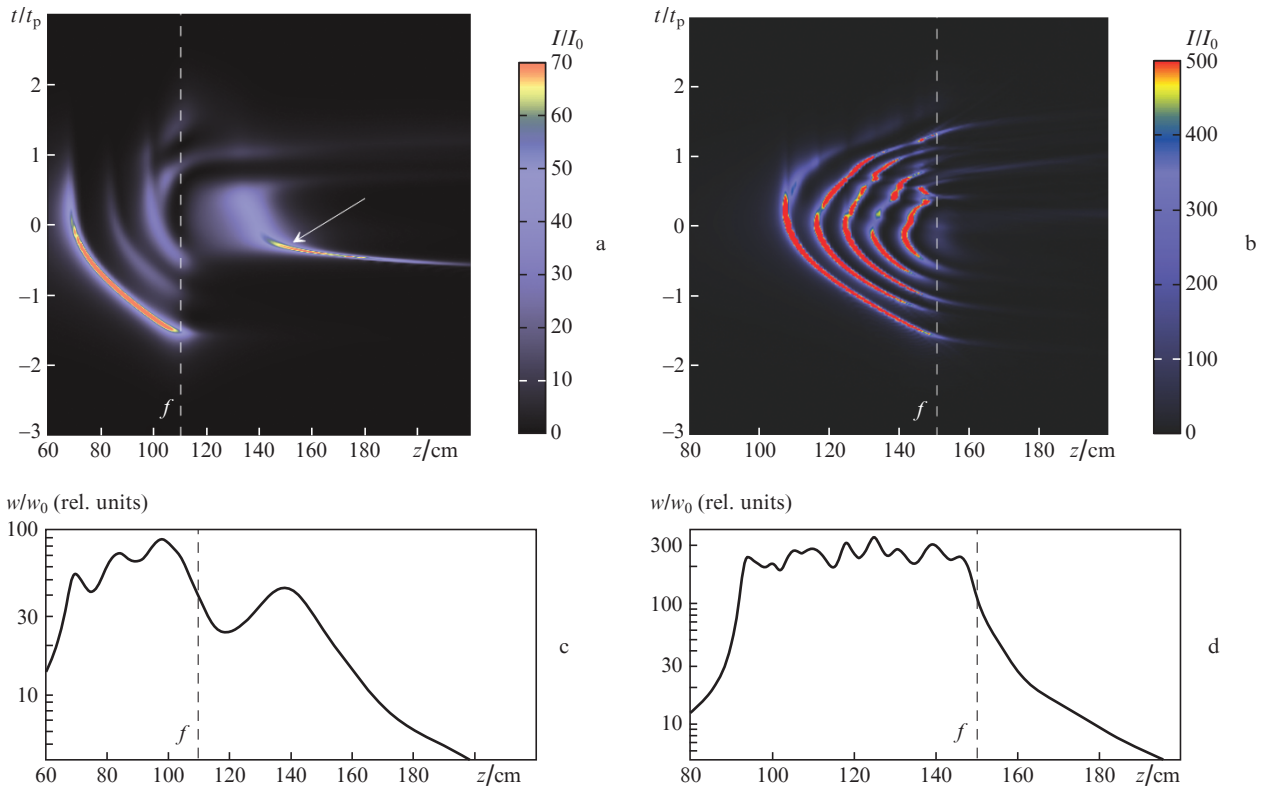

Figure 6. (a, b) Two-dimensional distributions of relative intensity $I(z, t)$ of focused pulsed (a) IR beams with $E_0 = 5.6$ mJ and (b) UV beams with $E_0 = 320$ μJ, propagating in air (the region of pulse refocusing is shown by an arrow), and (c, d) normalised energy density profiles along the path.

before the geometric focus of the beam. In addition, the intensity peaks for the third harmonic lie almost symmetrically with respect to the conditional pulse centre, whereas the nonlinear foci observed at filamentation of the fundamental harmonic are mainly shifted to the leading edge of the pulse. Note that several nonlinear foci can simultaneously be formed in different temporal layers of the pulse at a chosen optical-path point. These local intensity peaks have different amplitudes; actually, they are a manifestation of temporal pulse fragmentation in air [25], which is mainly caused by nonlinear refraction and absorption of the light beam in the plasma region formed by this beam.

After the passage through the focal waist the filamentation of both IR and UV beams ceases; however, the IR-beam filament is recovered thereafter and exists on a rather long path. It is noteworthy that the filament recovery begins again with the central temporal layer of the pulse.

Thus, we can suggest that the observed differences in the character of passing of UV- and IR-beam filaments through the focal waist are related to the specific features of plasma formation in the filament zone (specifically, with the energy spent on nonlinear multiphoton absorption in the medium and light wave defocusing in the newly formed plasma region). The degree of influence of these physical mechanisms on the filamentation dynamics is different for different spectral regions.

Short-wavelength UV radiation ionises air (for example, oxygen molecules O_2 as a result of three-photon absorption) more actively than the long-wavelength (IR) radiation of the same intensity; in the latter case, an ionisation event calls for absorption of eight photons [2]. Vice versa, defocusing of the optical wave by electron plasma is more efficient for the long-wavelength radiation, because the optical phase delay per unit path for a wave passing through this negative plasma 'lens', $\delta\varphi = k(n_0 - n_p)/n_0$ ($k = 2\pi/\lambda$ and n_p is the plasma refractive index) is proportional to the laser wavelength λ: $\delta\varphi = k\rho_e/(2\rho_c) \propto \lambda$. Here, ρ_c is the critical free-electron density [4]; plasma with a density exceeding this value is completely opaque for light.

Specifically this relationship between the nonlinear absorption and plasma refraction during pulse self-action is observed in Fig. 6 for the light spectral regions under consideration. High energy loss and strong temporal fragmentation of UV pulse in the filamentation stage exclude beam filamentation behind the geometric focus.

Indeed, Fig. 7, which shows the pulse intensity profiles directly in the centre of the linear focal waist and beyond it, evidently demonstrates that both pulses undergo temporal fragmentation during propagation to the geometric focus. However, this process is much more efficient for the third harmonic: a single UV pulse is transformed into a train of more than ten short (few femtoseconds) subpulses, which are well resolved in time. This temporal pulse shortening, first, sharply increases the destabilising effect of the frequency dispersion of the medium on the propagation of the entire train [26] and, second, reduces the energy and power

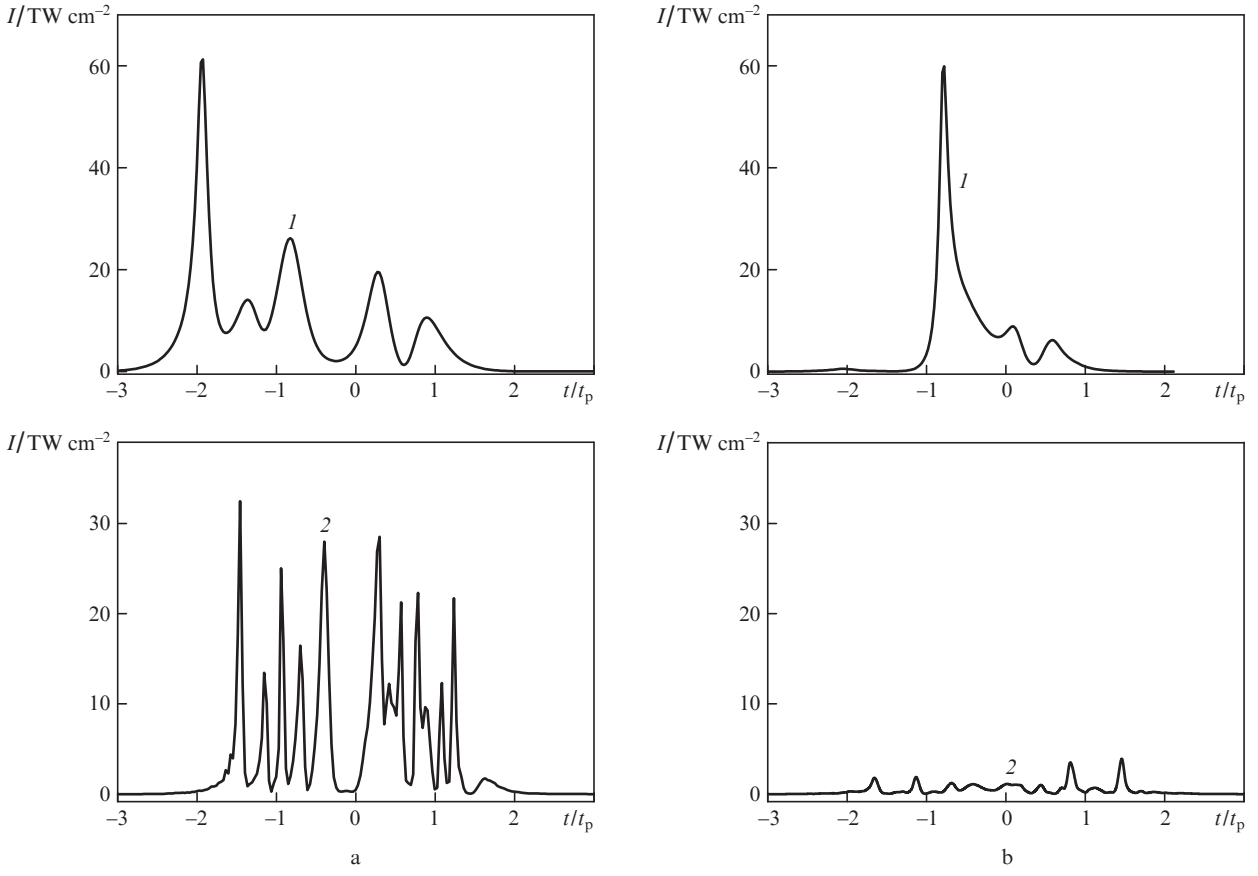

Figure 7. Temporal intensity profiles for (*1*) IR and (*2*) UV laser pulses (a) at the centre of the beam focal waist and (b) behind the geometric focus at $z = 160$ cm. The calculation parameters correspond to those in Fig. 6.

transferred by each subpulse. All these factors weaken the Kerr self-focusing of the pulse train, which cannot compensate for the diffraction divergence of the entire beam behind the geometric focus plane that sharply reduces the radiation intensity and leads to rapid termination of filamentation [Fig. 7b, curve (*2*)].

At the same time, the IR pulse is much less subjected to temporal time fragmentation, and the duration of individual subpulses is several times longer in this case. As a result, even despite the fact that the diffraction divergence of the IR beam emerging from the focus is several times larger than for the UV beam, the optical power of the virtual lens formed by the cubic nonlinearity of the medium successfully compensates for the diffraction divergence. A leading intensity peak is formed again near the temporal centre of the pulse on a rather short path segment [Fig. 7b, curve (*1*)], and the filament is recovered.

The total loss of the pulse energy on the ionisation of the medium and absorption in the formed plasma channel can be estimated based on the data of Fig. 8, which shows the relative change in the laser beam energy $\Delta E(z)/E_0 = [E_0 - E(z)]/E_0$ along the beam path for the two spectral regions. One can see that the loss of the IR pulse energy during filamentation is low: no more than 10% of the initial energy.

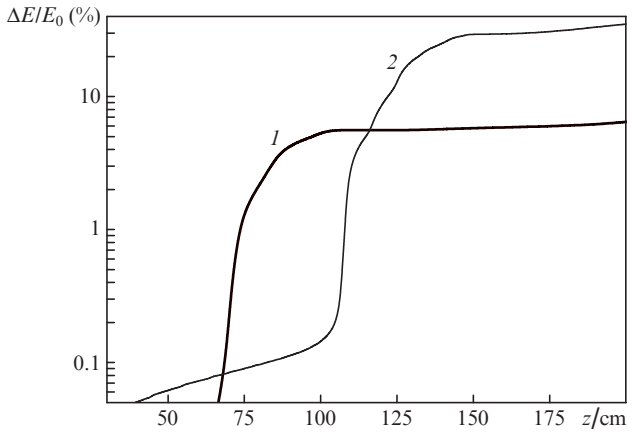

Figure 8. Relative change in the energy of (*1*) IR and (*2*) UV pulses along the propagation path. The calculation parameters are the same as in Fig. 6.

The UV pulse, due to the higher multiphoton absorption coefficient of air, loses ~30% of its initial energy by the instant of passage through the beam focal plane and up to 40% of energy by the end of the filamentation zone. As calculations show, almost all this energy is spent on the ionisation of the medium and the formation of a plasma channel with a high free-electron density on the beam axis. At the same time, the absorption of light in both near-IR and UV ranges in the plasma is very low (< 1%), because the peak values of free-electron density in the plasma channel are much smaller than the critical density ρ_c, which exceeds 10^{27} m^{-3} in the wavelength range under consideration. Therefore, the pulse energy loss on the air photoionisation can be an additional factor impeding the recovery of UV-beam filamentation behind the linear focus.

4. Conclusions

Thus, the complex study of the propagation of a focused pulsed laser beams in different spectral ranges (λ = 740 and 248 nm) in laboratory air in the self-focusing and filamentation regimes revealed the character of this process and the type of laser pulse filamentation behind the linear focal waist. The occurrence of beam filamentation behind the geometric focus was recorded by measuring the linear electron density in the plasma channel, the formation of which accompanies beam filamentation. It was found that a short-wavelength (UV) beam forms a plasma channel, which can, under certain conditions, continuously pass (be extended) behind the geometric focus of the beam. Post-focal filamentation of the IR beam is generally implemented as refocusing, which is characterised by a pronounced decrease in the free-electron density in the plasma channel directly behind the geometric focus and its subsequent recovery practically to the previous level at a larger distance. At the same time, it is much more difficult to implement experimentally filamentation of UV laser beam behind the linear focus by varying the lens focal length, the beam transverse size and the beam power than in the case of IR-beam filamentation. This can be done either by using sufficiently narrow beams or by increasing significantly the pulse power and implementing the multiple filamentation regime. The numerical simulation of the self-action of focused UV and IR laser pulses in air showed that the revealed differences in the beam filamentation behind the geometric focus may be related to a significant energy loss on the photoionisation of the medium and stronger temporal fragmentation of UV pulse before the focal waist, which is an additional hindrance for its subsequent post-focal filamentation.

Acknowledgements. This work was supported by Fundamental Research Programme No. 13 of the Presidium of the Russian Academy of Sciences, Integration Project No. 67 of the Presidium of the Siberian Branch of the Russian Academy of Sciences, the Russian Foundation for Basic Research (Grant Nos 12-05-00716-a, 09-05-00738-a, 11-02-12061, 10-02-01477, and 11-02-01100) and the International Science and Technology Centre (Grant No. 4073).

References

1. Shen Y.R., Boyd R.W., Lukishova S.G. (Eds) *Self-focusing: Past and Present* (New York: Springer, 2009).
2. Berge L., Skupin S., Nuter R., Kasparian J., Wolf J.-P. *Rep. Prog. Phys.*, **70**, 1633 (2007).
3. Kandidov V.P., Shlenov S.A., Kosareva O.G. *Kvantovaya Elektron.*, **39**, 205 (2009) [*Quantum Electron.*, **39**, 205 (2009)].
4. Couairon A., Myzyrowicz A. *Phys. Rep.*, **441**, 47 (2007).
5. Tzortzakis S., Prade B., Franco M., Mysyrowicz A. *Opt. Commun.*, **181**, 123 (2000).
6. Mechain G., Amico C.D., Andre Y.-B., Tzortzakis S., Franco M., Prade B., Mysyrowicz A., Couairon A., Salmon E., Sauerbrey R. *Opt. Commun.*, **247**, 171 (2005).
7. Berge L., Skupin S., Lederer F., Méjean G., Yu J., Kasparian J., Salmon E., Wolf J.P., Rodriguez M., Woste L., Bourayou R., Sauerbrey R. *Phys. Rev. Lett.*, **92**, 22502 (2004).
8. Hosseini S.A., Luo Q., Ferland B., Liu W., Chin S.L., Kosareva O.G., Panov N.A., Aközbek N., Kandidov V.P. *Phys. Rev. A*, **70**, 033802 (2004).
9. Durand M., Houard A., Prade B., Mysyrowicz A., Durécu A., Moreau B., Fleury D., Vasseur O., Borchert H., Diener K., Schmitt R., Théberge F., Chateauneuf M., Daigle J., Dubois J. *Opt. Express*, **21**, 26836 (2013).

10. Point G., Brelet Y., Houard A., Jukna V., Milián C., Carbonnel J., Liu Y., Couairon A., Mysyrowicz A. *Phys. Rev. Lett*., **112**, 223902 (2014).
11. Vlasov S.N., Talanov V.I. *Samofokusirovka voln* (Wave Self-Focusing) (Nizhny Novgorod: Izd-vo IPF RAN, 1997).
12. Lange H.R., Grillon G., Ripoche J.-F., Franco M.A., Lamouroux B., Prade B.S., Mysyrowicz A. *Opt. Lett*., **23**, 120 (1998).
13. Talebpour A., Petit S., Chin S.L. *Opt. Commun*., **171**, 285 (1999).
14. Kosareva O.G., Kandidov V.P., Brodeur A., Chin S.L. *J. Nonlinear Opt. Phys. Mater.*, **6**, 485 (1997).
15. Brodeur A., Chien C.Y., Ilkov F.A., Chin S.L., Kosareva O.G., Kandidov V.P. *Opt. Lett.*, **22**, 304 (1997).
16. Geints Yu.E., Zemlyanov A.A., Kabanov A.M., Matvienko G.G., Stepanov A.N. *Opt. Atmos. Okeana*, **25**, 745 (2012).
17. Askar'yan G.A., Dianov Kh.A., Mukhamadzhanov M. *Pis'ma Zh. Eksp. Teor. Fiz.*, **14**, 452 (1971).
18. Geints Yu.E., Zemlyanov A.A., Izyumov N.A., Ionin A.A., Kudryashov S.I., Seleznev L.V., Sinitsyn D.V., Sunchugasheva E.S. *Zh. Eksp. Teor. Fiz*., **143**, 228 (2013).
19. Fedorov V.Yu., Kandidov V.P. *Opt. Spektrosk.*, **105**, 291 (2008).
20. Dergachev A.A., Ionin A.A., Kandidov V.P., et al. *Kvantovaya Elektron.*, **43**, 334 (2013) [*Quantum Electron*., **43**, 334 (2013)].
21. Kosareva O.G., Liu W., Panov N.A., Bernhardt J., Ji Z., Sharifi M., Li R., Xu Z., Liu J., Wang Z., Ju J., Lu X., Jiang Y., Leng Y., Liang X., Kandidov V.P., Chin S.L. *Laser Phys*., **19**, 1776 (2009).
22. Geints Yu.E., Zemlyanov A.A. *Laser Phys.*, **23**, 035301 (2013).
23. Perelomov A.M., Popov V.S., Terent'ev M.V. *Zh. Eksp. Teor. Fiz*., **50**, 1393 (1966).
24. Couairon A., Berge L. *Phys. Rev. Lett*., **88**, 135003 (2002).
25. Mlejnek M., Wright E.M., Moloney J.V. *Opt. Lett*., **23**, 382 (1998).
26. Moll K.D., Gaeta A.L. *Opt. Lett*., **29**, 995 (2004).